Proceedings of IJTC2006
STLE/ASME International Joint Tribology Conference
October 22-25, 2006, San Antonio, TX, USA

IJTC2006-12095

Laser Glazing Process Development and Optimization for Railroad Applications*

S. H. Aldajah, O. O. Ajayi**, and G. R. Fenske**
United Arab Emirates University
Al-Ain, UAE
**Energy Technology Division
Argonne National Laboratory
Argonne, IL 60439

Railroad industry is very important to the U.S. Nearly 60% of the U.S. freight is transported by railroads. Fuel represents about 9.5 percent of the operating cost of a railroad; the industry is aggressively trying to find ways to improve fuel efficiency. One major contributor to the railroad energy losses is the friction between the wheel and the rail. Many technologies have been implemented to reduce the high friction between the wheel and the rail. Such technologies include the application of liquid lubricants as oil and grease to the gage side of the rail. Such lubricants, wash away in the rain, introduce environmental problems, and may cause a train to lose traction if they migrate to the top of the rail. On the other hand, a new technology has recently been developed at Argonne National Laboratory (ANL) showed desirable results. This technology involves the use of laser to treat (glaze) the gage side of the rail. Treating steel rails by "laser glazing" reduces friction between the rails and train wheels by approximately 60%, which may reduce rail cracking by up to 75%. Reducing friction can save an estimated $60 million in fuel costs and $16 million in rail replacements, as well as lower the risk of derailment. This paper focuses on the optimization of the laser glazing process for the railroad applications.

*Work supported by the Department of Energy, Office of Transportation Technology, under Contract W- 31-109-Eng-38.

Introduction

Wheel-rail friction could be both friend and foe. It is essential during the pulling process and without it, braking system couldn't bring train to a stop. However, the friction between the car wheels and the rail while rolling is undesirable. It is a contributor to energy wastage and damage caused in railroads. The heavy freight trains are rolling on the basis of a wheel set, which consists of two wheels connected to a rigid axle; therefore, in order to roll forward on a curve, at least one wheel encounters a small slip. This slip is in both longitudinal and lateral directions and it produces very undesirable friction forces. The lateral forces produced in this way have been measured in the field and found to be between 15,000 – 20,000 lb/axle (sometimes more) [1] The total lateral force developed on a test train was measured to be as high as 5,000,000 lb on a curve [2] This excessive force can roll over the rail resulting in a catastrophic derailment. Even otherwise, it produces large wear and damage to both the rail and track as well as to the wheels. The problem has been exacerbated in the last two decades because of the increase in axle loads (as high as 36 tons/axle) resulting in high loads and contact stresses.

The current practice today to alleviate some of the friction and wear problems is by applying grease to the wheel flanges or the gage corner of the rail. This results in friction reduction but it may cause a train to lose traction if the grease migrates to the top of the rail.

Laser glazing, on the other hand, is a promising technology that can be applied to the railroad tracks. Rail laser glazing is based on the principle that a harder material generally causes less friction. It involves melting the surface of the rail by a laser and letting it solidify quickly to form a hard and smooth glassy surface that is elastic enough to

distribute load evenly to the underlying layer. Laser glazing forms the equivalent of a solid-state lubricant that stays where it is applied and is environmentally benign. Laser glazing process increases wear resistance, reduces friction coefficient and increases rolling contact fatigue resistance.

The primary task of this project was to optimize the laser glazing process and to conduct laboratory and field friction and wear tests with glazed and unglazed surfaces.

The concept of Laser Glazing

Recent advances in the Nd:YAG (neodymium-yttrium aluminum garnet), excimer, and CO_2 lasers have made possible a wide range of applications and emerging technologies in the computer, microelectronics, and materials fields. In the field of materials processing, surface treatments and surface modification for metals and semiconductors are of particular interest. With appropriate manipulation of the processing conditions (e.g., laser power density or interaction time), a single laser can be used to perform several processes. There are many techniques for the surface modification of materials, as listed in Table1. However, surface modification by laser has several advantages, among them the ability to produce a fine-grained structure, low porosity, relatively smooth surface, low heat-affected zone in the substrate, and good bonding between the coatings and substrate.

Table 1 Surface Modification Techniques

Typical Established Processes	**New Techniques**
Hot Dip Molten Metal	Chemical Vapor Deposition (CVD)
Electroplating	Physical Vapor Deposition (PVD)
Diffusion Process	Laser
Plasma Spraying	Ion Beam Mixing
Vacuum Evaporation Deposition	Ion Implantation
	Ion Plating

Laser Glazing

In laser glazing, a small fraction of the top surface of a material is melted and rapidly solidified to develop new microstructures. This technique is often used to seal the surface of plasma-deposited thermal barrier coatings on a nickel substrate to improve high-temperature corrosion properties. The pulsed laser has been extensively used in the electronics industry for the glazing of semiconductors. Laser glazing has also received considerable attention as a method to improve the surface properties of the substrate such as wear, corrosion, and fatigue resistance. Glazing can be done either with pulsed or continuous-wave lasers.

A pulsed laser provides a means of achieving very rapid heating (melting) and cooling (solidification) of the surface. A wide range of quenching rates is achievable, and high quenching rates (10^6-10^{16} K/ s) are possible when various laser process parameters are utilized [3] Controlled laser energy and rapid quenching have been used to produce perfect recrystallized surface layers.

In the laser glazing process, laser energy is absorbed by the surface of the solid, it melts the surface, and the melt front propagates into the bulk to a depth determined by deposited energy and material parameters. The melt velocity is controlled by the rate of energy deposition, the absorbed depth in the solid and liquid phases and thermal properties of the solid. After the surface has been melted, the molten layer resolidifies as heat flows into the underlying substrate. Resolidification occurs at the liquid-solid interface. Because of high temperature gradients, the resolidification velocity can be very large. Temperature gradients ($\delta T/\delta Z$) of up to 10^9 K/cm and corresponding quench rates of up to 10^{11} K/s can be readily achieved [4].

Process development. This effort primarily focused on laser glazing, a process that involves producing a thin molten layer on the surface, in contrast to laser hardening, in which no melting occurs. The project was initiated by Ron DiMelfi and much of the initial research and process development was performed by ANL's Laser Applications Laboratory (initially directed by Keng Leong, later, by Claude Reed and Zach Xu). The most recent laser glazing activities (in preparation for full scale tests) were performed by NuVonyx [5]. Initial glazing activities at ANL involved parametric studies to optimize the conditions under which a glazed layer forms on 1080 steel when an Electrox 1.6-kW pulsed Nd:YAG laser with fiber-optic beam delivery and special beam shaping optics. In the early studies, two approaches were developed: one that involved a single pass of the laser over a given area, and one that involved multiple overlapping passes, Figure 1. The Knoop hardness of the martensitic glazed regions was 2-3 times greater than that of the substrate, depending on whether a single-pass (factor of 3 times harder) or multipass (slightly over 2 times harder) process was used.

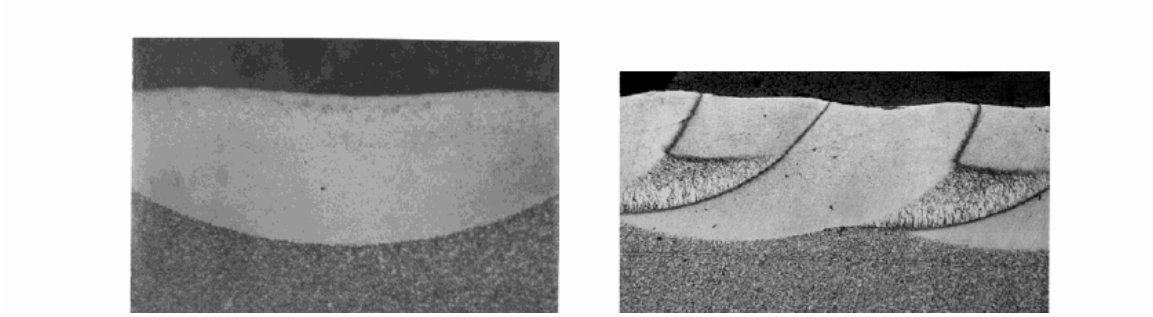

Figure 1 a: Single Pass Laser Glazed Cross Section, b: Multi Pass Laser Glazed Cross Section

The initial ANL efforts were performed at relatively slow glazing speeds (5 mm/s) and produced rough surfaces (see Figure 2). Later attempts to operate at higher glazing speeds (10 mm/s) produced smoother surfaces (Figure 2b). A commercial laser glazing process that utilized high-power diode laser technology was also investigated. In this case, bars of 108 steel were processed by a commercial vendor (NuVonyx -http://www.nuvonyx.com/) and subsequently tested at ANL (Figure 3a). A third modification of the process (laser shot-peening (LSP)) was also evaluated. Bars of 1080 steel were processed by LSPT (LSP Technologies) to 'peen' near-surface regions (Figure 3b). LSP does not involve melting near-surface regions; instead, it utilizes a laser to shock near-surface regions, thereby introducing high compressive stresses and increasing hardness.

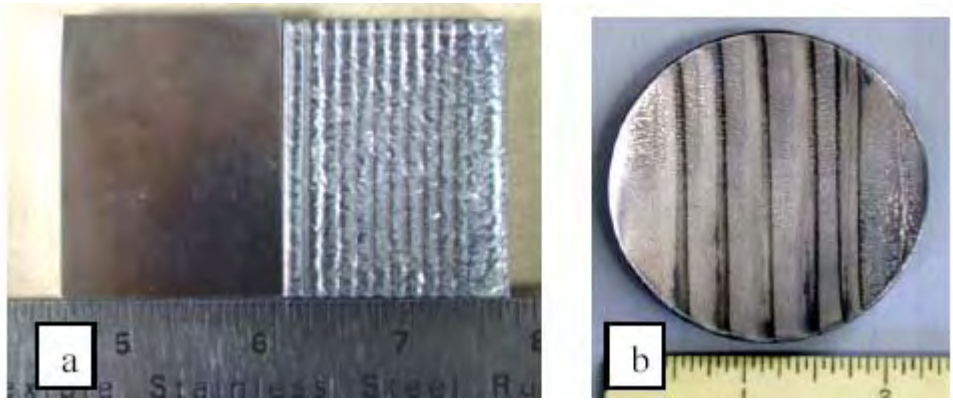

Figure 2 Glazed steel: (a) 5 mm/s, and (b) 10 mm/s

Friction and wear. Tests of friction and wear were performed on laser-treated coupons (primarily ANL-glazed steels) to evaluate the potential of glazing to reduce frictional losses between the wheel flange and the gauge face of the rail. Initial tests were performed at Falex Corporation in a low-speed block-on-ring configuration [6], and at the (AAR) test facility in Pueblo, CO with a full-scale ring/wheel-on-block/rail, operated under controlled slip conditions. Detailed tests were performed at ANL on twin-roller, pin-on-disc (POD), and reciprocating pin-on-flat configurations. The block-on-ring tests at Falex measured the breakaway (e.g., static friction coefficient) torque/force required to initiate rotation (defined as 0.013 rpm) under various loads (445- 4005 N [100-900 lb]) in 100-lb (445-N) increments. (The ring in this case was a Falex standard ring, 'S-10 steel' with a Rc of 58-63; the block was 1080 rail steel, as-received or glazed.) Dynamic block-on-ring tests were not performed because earlier tests showed that debris accumulation produced unreliable comparisons under dry, heavily loaded conditions. The Falex test results showed static friction coefficients for untreated 1080 of ¡Ö 0.35-0.45, which dropped to values that ranged from 0.2 to 0.4 for differing glazing conditions.

Figure 3a: 1080 steel glazed with high-power diode laser, b: 1080 steel laser peened (right side) and glazed and peened (left side)

The AAR tests were similar to the Falex tests in that they measured the breakaway friction (friction to start rotation) and the friction during maintained rotation, but on a much larger scale. The AAR tests were performed on a segment of rail that was glazed on the top of the rail; the top of the rail was subjected to pure rolling and, at the end, to rolling/sliding contact, Figure 4. The static friction coefficient of the untreated 1080 rail varied from 0.2 to 0.5, depending on the applied load, whereas the friction coefficient of the glazed regions varied from 0.1 to 0.25. Dynamic friction coefficients for the glazed regions varied from 0.2 to 0.35, depending on load, compared to 0.2 to 0.55 for unglazed regions.

The benchtop tests at ANL were more controlled than the full-scale tests at the AAR facilities. The environment was more repeatable in terms of surface contaminants and more consistent in terms of relative humidity, two factors that significantly affect the frictional response. The POD tests used flats of 1080 steel, glazed and unglazed, that rubbed against stationary balls or pins (52100, 1080 steel, 440C, or alumina). The tests revealed that the composition of the pin/ball significantly affected the friction coefficient

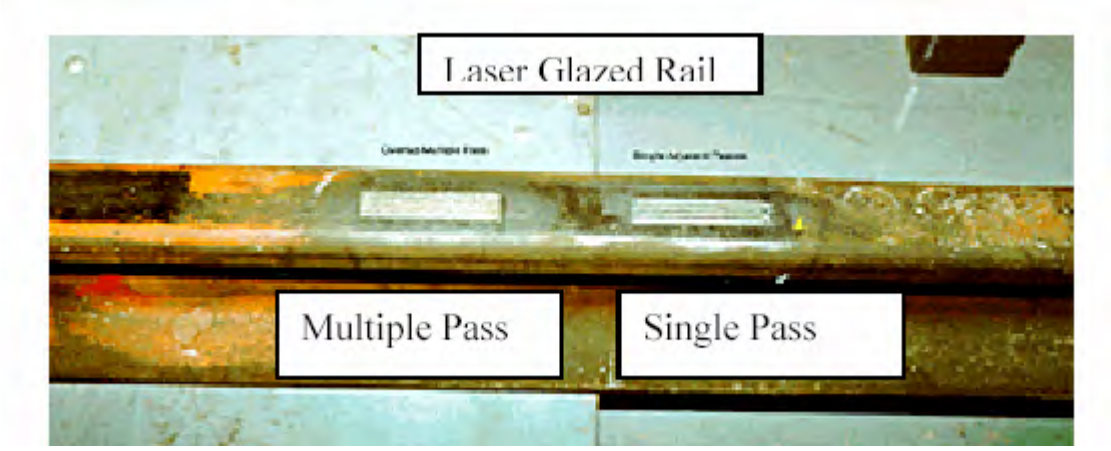

Figure 4. Segment of laser-glazed 1080 rail used in AAR friction tests

Figure 5. The general trend was that the glazing reduced the friction coefficient by 3-35%, depending on the material. The greatest reduction was for an alumina ball sliding against the 1080 steel, suggesting that a strong chemical adhesion mechanism may be active with the metallic counterparts.

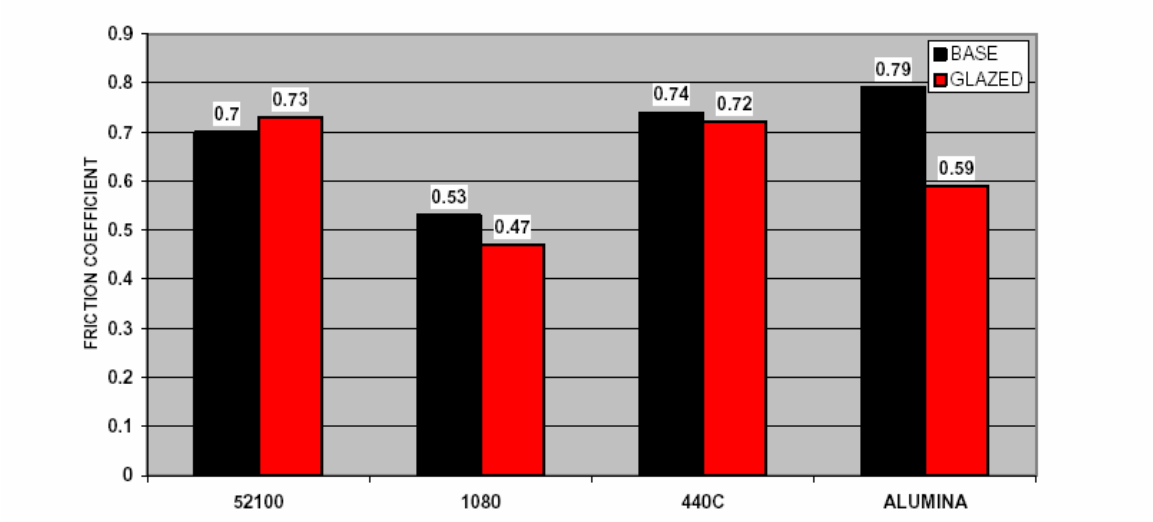

Figure 5. POD friction coefficients of glazed and unglazed steel sliding against various pin materials under dry sliding [7].

A twin-roller test configuration, Figure 6, was also used to more closely simulate the rolling contact stresses present at wheel/rail interfaces. The system shown in Figure 6 was used extensively to simulate the stresses present in 100-ton rail cars. The system is configured to measure the lateral friction forces. Tests were performed with 1045 steel rail and wheel discs that were through-hardened (Rc 40) or glazed. The glazing effectively reduced the friction coefficient from roughly 0.4 for the unglazed condition to 0.3 for the glazed rail rotating on an unglazed 1045 steel counterpart, Figure 7.

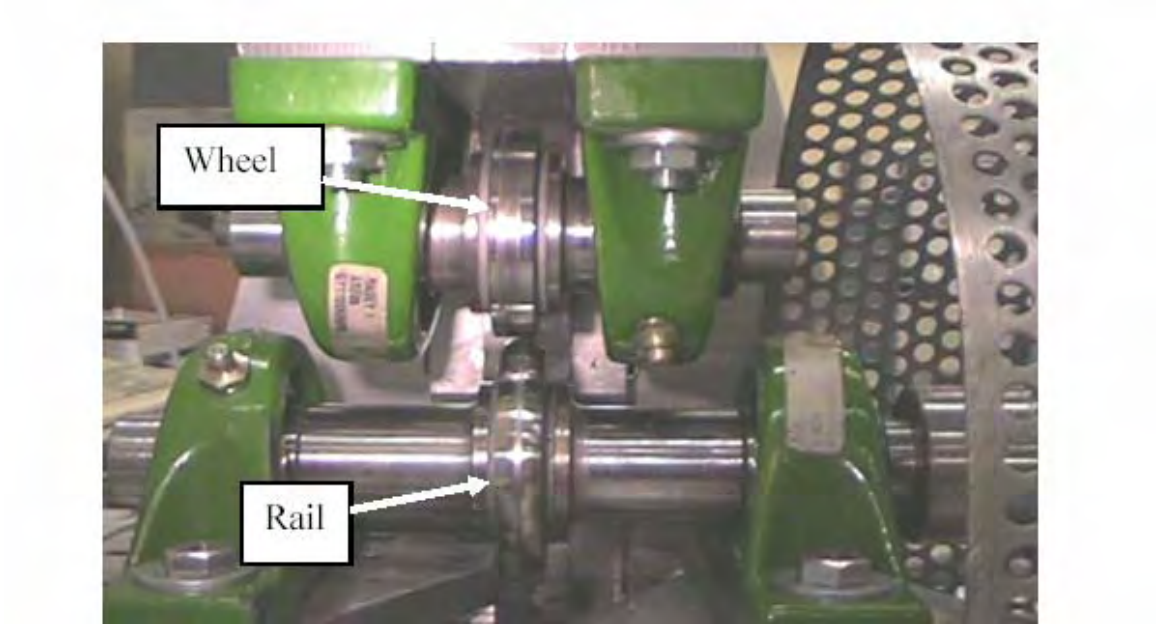

Figure 6. Photograph of LA-4000 twin-roller test rig used to simulate high-contact stresses

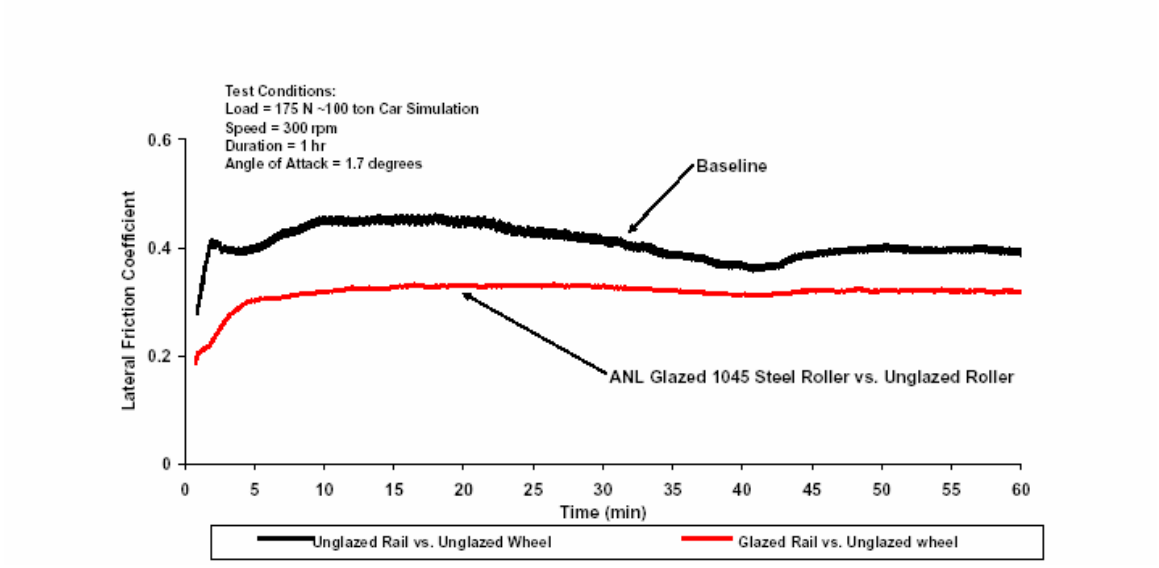

Figure 7. Twin-roller friction data on glazed and unglazed 1045 steel

Similar tests were performed on 1045 steel rollers that were treated with a diode laser by a commercial vendor (NuVonyx). The NuVonyx-treated samples also exhibited lower

friction than the untreated steel; however, the low-friction behavior did not endure for as Rail Wheel.

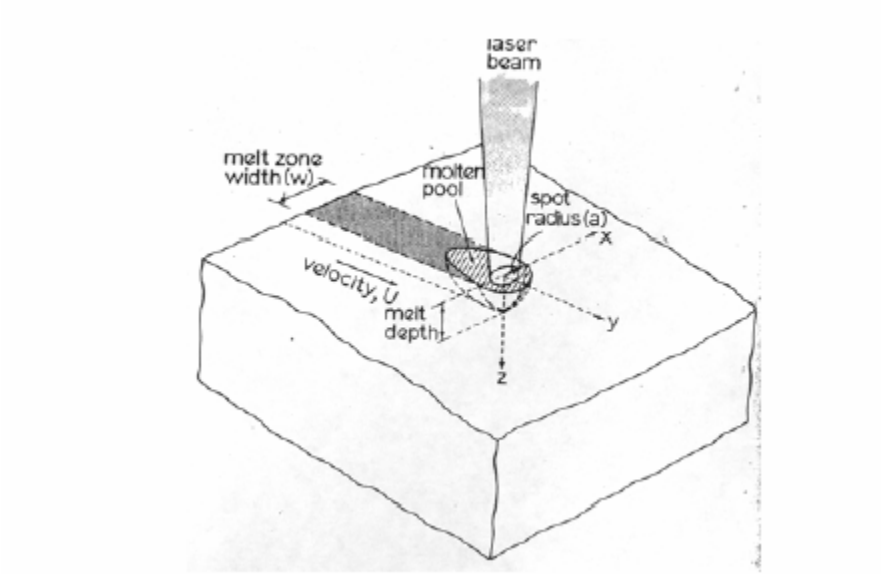

Figure 8. Schematic illustration of laser beam substrate geometry during rapid surface melting and solidification

long as that of the ANL-treated coupons. The difference in endurance is due in part to the fact that the NuVonyx laser treatment was not as well optimized as the ANL treatment.

Tests were also performed to evaluate the durability of the glazed region, in particular to determine if the glazed region would delaminate from the underlying steel. This is a major concern for railroad applications because delamination could be a precursor to the formation of cracks that lead to rail degradation. Long-term (24-48-h) twin-roller tests at a high angle of attack were performed on the twin-roller rig shown in Figure 6. A 24-h test simulates the passage of ¡Ö1100 100-car trains (each loaded at 100 tons). In all cases, the glazed region remained intact and showed no evidence of delamination.

Microstructural characterization. The microstructure of glazed steel coupons was characterized to determine if a ‘white layer’ was produced that could account for the

reduced friction. Optical and electron microscopy (both scanning and transmission microscopy [SEM and TEM]) were used to characterize the microstructure. Microhardness was also measured, as a function of depth into the substrate in the glazed regions.

Laser treatment of engineering material to modify the surface properties is now a common industrial practice. Surfaces of steel material can easily be heat hardened with a laser beam. Laser glazing, in which the temperature is high enough to melt a region in the surface (as shown schematically in Figure 8), is a variation of surface thermal treatment. The melt zone is surrounded by a heat-affected zone in which the temperature is quiet high but not up to the melting point. This surface heating and melting is then followed by a very rapid cooling, leading to rapid solidification of the molten surface layer.

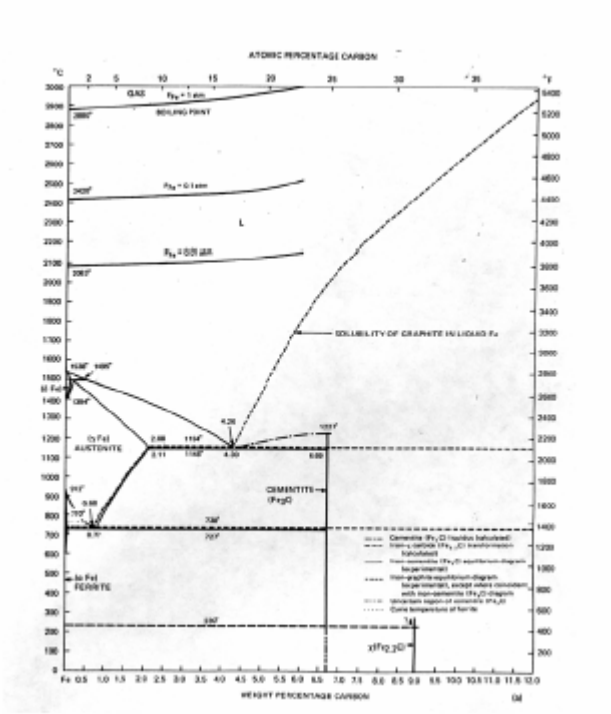

Figure 9 Carbon-iron phase diagram showing eutecoid region; ferrite field, including quilibrium Fe- C, Fe-Fe3C, Fe-Fe2.4C, and delta ferrite field. (J. Chipman, Metals Handbook, 8th ed., vol. 8, Am. Soc. Met., Metal Park, Ohio, 1973, with permission)

The microstructural evolution in the laser-glazed layer on 1080 carbon steel surface can be understood from the Fe-C phase diagram shown in Figure 9, and from the rapid solidification process in plain carbon steel such as 1080. From Figure 9, we see that the temperature in the melt zone for 1080 steel is greater than 1500°C. Materials in the region below this melt zone (with temperatures between 730 and 1500°C and designated the heat affected zone) are transformed into austenite phase. Materials with a temperature below 730°C retain the original pearlitic microstructure of their base material. With the very rapid cooling (cooling rates of 103-106 KS-1 have been suggested by [8] of the laser glazing process, the now austenite phase of the heat-affected zone will be transformed to martensite. The liquid pool of the melt zone will also be supercooled and will undergo a nonequilibrium rapid solidification process, producing a somewhat complex microstructure. Two review papers on weld solidification and rapid solidification provide some insight into possible microstructural evolution when the melt zone during laser glazing solidifies, [7, 9].

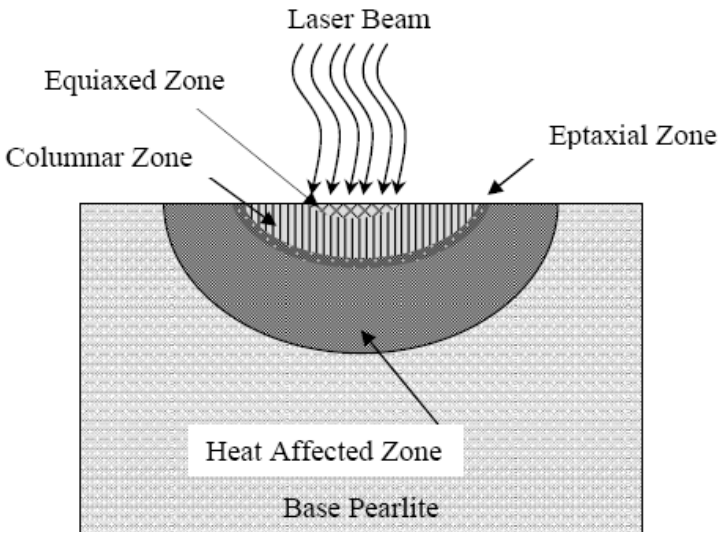

Figure 10. Schematic of microstructural evolution during laser glazing of 1080 carbon steel surface

Because of the rapid solidification involved, the composition of the melt as it solidifies remains the same as the base composition, because the time for solute segregation is not sufficient. Also, because the melt pool is in contact with solid material of the same composition, the initial solidification occurs expitaxially in the grains of the base metal. As solidification progresses, some grains with preferred easy growth direction may grow at a faster rate, producing a columnar grain structure. Finally, in the center region, lastto-solidify homogeneous nucleation of new grains is sufficiently easy to allow formation of an equiaxed grain structure. High nucleation density expected in the supercooled region in the center is also expected to produce fine grains. Thus, the microstructure of the center region consists of very fine equiaxed grains.

As the melt zone solidifies, a solid austenite phase is formed, regardless of the grain morphology. Because the cooling rate in the newly solidified region is still high, the "new" austenite is also expected to transform into martensite. Thus, the expected microstructure of the glazed layer on 1080 steel is martensite, but derived from three or four different types of austenite grains. In the heat-affected, unmelted zone, the martensite is derived from the austenite form in the solid state in the base material. In the austenite formed from the melt zone, there is a very thin layer of expitaxial grains, followed by columnar, grains, and finally, fine equiaxed grains at the centerline surface.

A schematic illustration of these various zones and regions is shown in Figure 10.

Samples of glazed 1080 were prepared for the characterization of the microstructure of the glazed layer. Specimens were cut, mounted in bakelite and polished by the conventional metallographic sample preparation technique. The samples were first etched in Vilella's reagent (5% HCl, 95% methanol, 1 g picric acid) to reveal the outline of prior

austenite grains in the glazed layer. The samples were later etched in 2% Nital to show the final phases present in the surface layer.

Figure 11 shows the optical photomicrograph of the glazed layer etched in Vilella's reagent to reveal the prior austenite grain boundaries. The austenite grain morphology is consistent with the schematic diagram of Figure 10. A very narrow region of epitaxial Laser

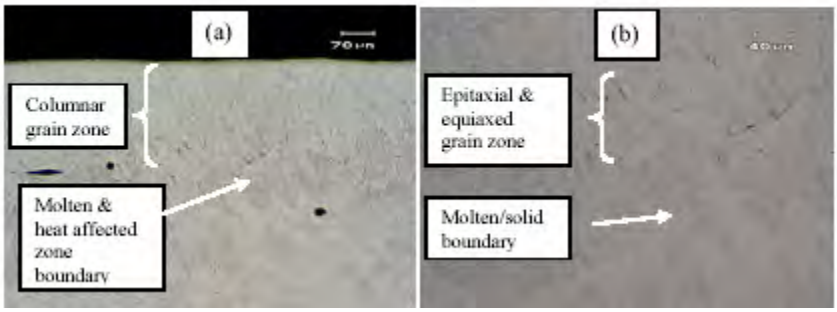

Figure 11. Optical photomicrograph at (a) lower and 9b) higher magnification of laser-glazed layer etched with Vilella's reagent to show outline of previous austenite grain boundaries. (a) columnar morphology of top layer as molten layer solidifies and (b) boundary region between heat-affected zone and molten zone with initial expitaxial grain as solidification begins

equiaxed grains invisible at the boundary of the heat-affected zone and the melt zone, as indicated by the photomicrograph at higher magnification, shown in Figure 11b. On top of this narrow region is the columnar-grain zone, followed by a very narrow equiaxed-grain layer at the very top surface. Upon the rapid cooling involved in the laser glazing process, all of the austenitic phases that were formed in both the heat-affected zone and the rapidly solidified molten zones (regardless of the austenite grain morphology) are transformed into martensite, as indicated in Figure 12, optical photomicrograph of the sample etched with 2% Nital. Indeed, after this phase transformation, it is difficult to distinguish between martensite formed from the solidified-molten-layer austenite and the

solid-state heat-affected-zone austenite.

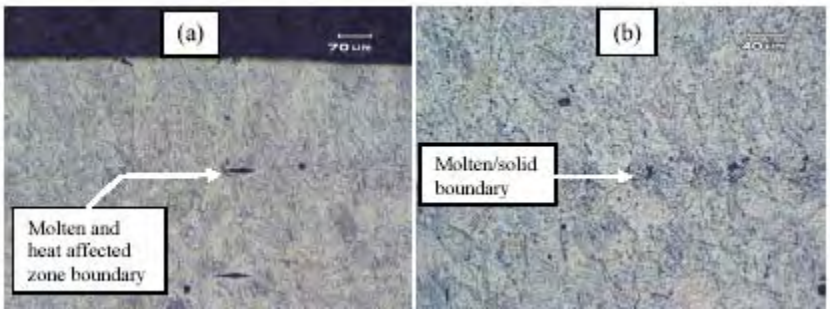

Figure 12. Optical photomicrograph of glazed layer etched with 2% Nital, showing that final phase in both molten and heat-affected zones consists of martensite. (a) top layer of the molten zone and (b) boundary between molten and heat-affected zones.

Microhardness. The microhardness of samples produced by the ANL and NuVonyx processes was characterized as a function of depth. Figure 13, [10], shows SEM cross sections of ANL-glazed (single-pass and overlapped) rail. The single-pass Columnar (nonoverlapped) glazed region registered Knoop hardnesses that ranged from approximately 900 at the surface to a peak value of 1075 further in; in the base steel, the values dropped to 350-400. When the beams are overlapped, some degree of tempering occurs. The results were very consistent from sample to sample, even between samples produced by the ANL process and the NuVonyx process.

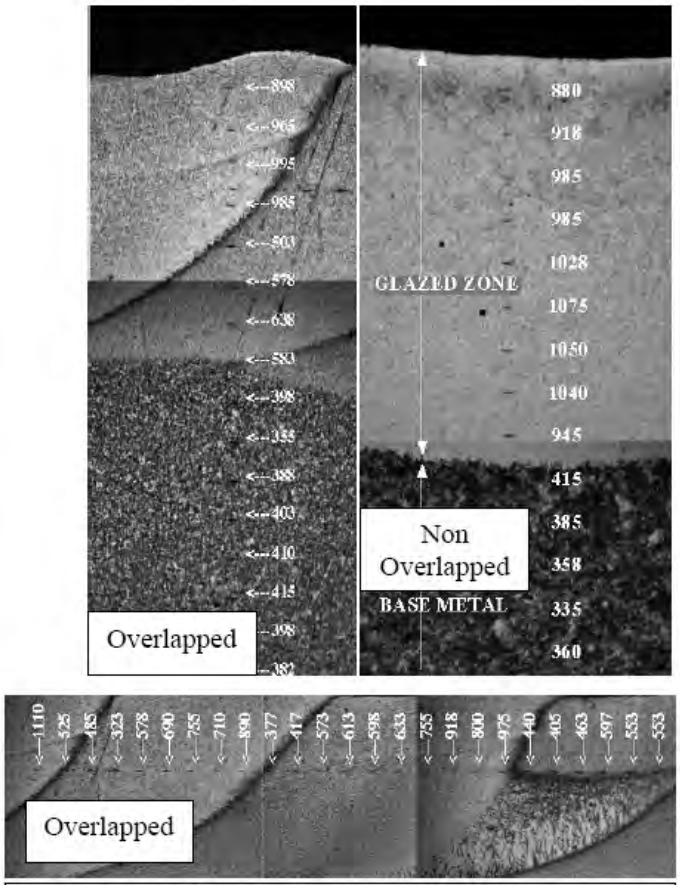

Figure 13. SEM photomicrographs of ANL-glazed rail steel illustrating variation of Knoop hardness with position.

Figure 14 shows the hardness of a series of 1080 steel bar samples that were treated by the NuVonyx process (4 kW, at two speeds, 2 and 2.5 m/s). The hardness of the 1080 substrate was 350-400 Knoop, increasing to ¡Ö1100 Knoop, decreasing to 800-900 Knoop near the surface. The glazing process, whether ANL or NuVonyx, produces a hard martensitic phase on top of the base pearlitic 1080 steel. The main difference between the two processes appears to be the thickness of the treated layer. The thickness of the treated region is inversely proportional to the speed. Higher laser-translation speeds produce glazed regions that are thinner, as shown in Figure15.

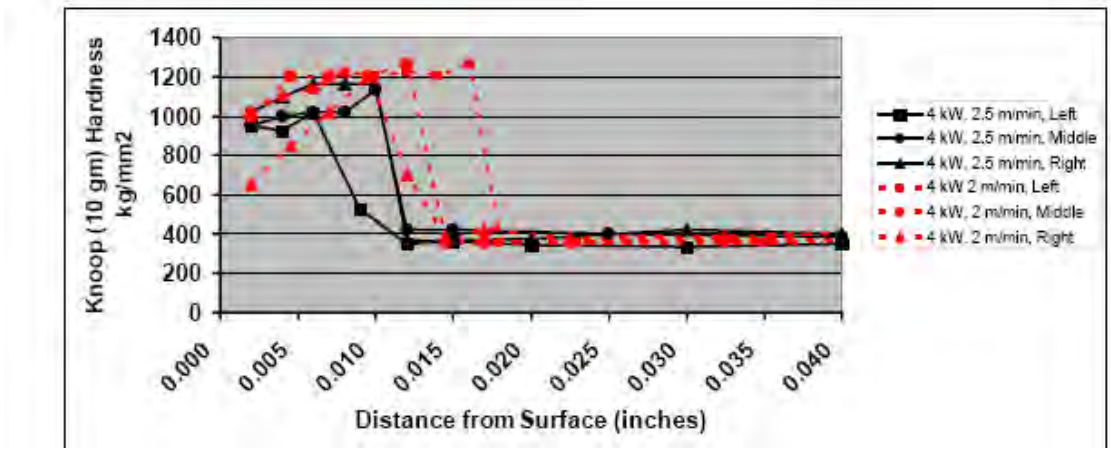

Figure 14. Knoop (10-gm) microhardness of NuVonyx-glazed steel

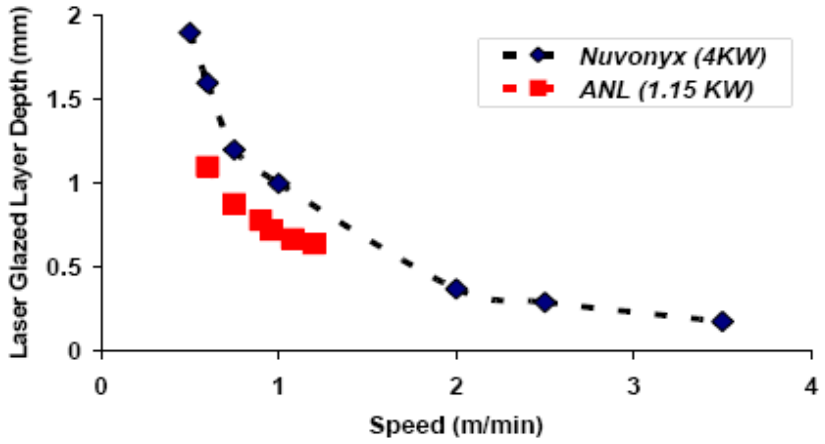

Figure 15. Depth of laser-treated zone as a function of laser speed

Laser Glazing of Rim (NuVonyx)

In preparation for the Ottawa full scale tests, two rim segments (each rim is comprised of two 180˚ segments bolted onto a central hub) were sent to ANL for laser glazing. One segment was used by NuVonyx to optimize their laser processing protocol to produce a glaze comparable to those produced at ANL. This segment was subjected to several glazing treatments and sectioned for metallographic examination (hardness and microstructure).

The second 180˚ segment was glazed over a 175˚ arc and was re-assembled with the original mating segment on rim 'A' in Figure 2.

The original plan was to glaze the pink-shaded region of the rim as shown in Figure 3. For these tests, the glazed region started at the gauge point and was to extend approximately 2-in. onto the top of the rim/rail. In practice, the glazing would not extend this far onto the top of the rail (to avoid potentially low friction on the top of the rail, where traction is critical), but for the purposes of these tests, a wider swath was selected to ensure contact between the wheel and glazed region on the rim.

Because the existing laser facilities at NuVonyx were not adequate to glaze a single 2-in.-wide swath in one pass on the curved rim segment, as illustrated in Figure 3, we decided to develop a multipass process that would glaze a 2-in.-wide swath by overlapping swaths that were ½-in. wide. Initial tests with 1080-steel coupons and a short segment of 'virgin' 1080 rail suggested multipass (overlapped) glazing was viable, and NuVonyx proceeded to perform a series of glazing experiments on the sacrificial rim segment to optimize the glazing process. Glazing trials were performed under various conditions (speed, laser power, and beam size) to determine the optimum conditions needed to form a glazed region that was approximately 1-1/2 mm deep; the results presented in Figure 4A indicate that, at a power level of 4 kW, a translation speed of approximately 0.6 m/min was required. Knoop microhardness data for a series of runs performed at 0.6 m/min on the sacrificial rim are shown in Figure 4B. As seen in Figure 4B, the depth of the hardened zone ranged from approximately 1.5 to 2 mm. The surface hardness was approximately 800 Knoop.

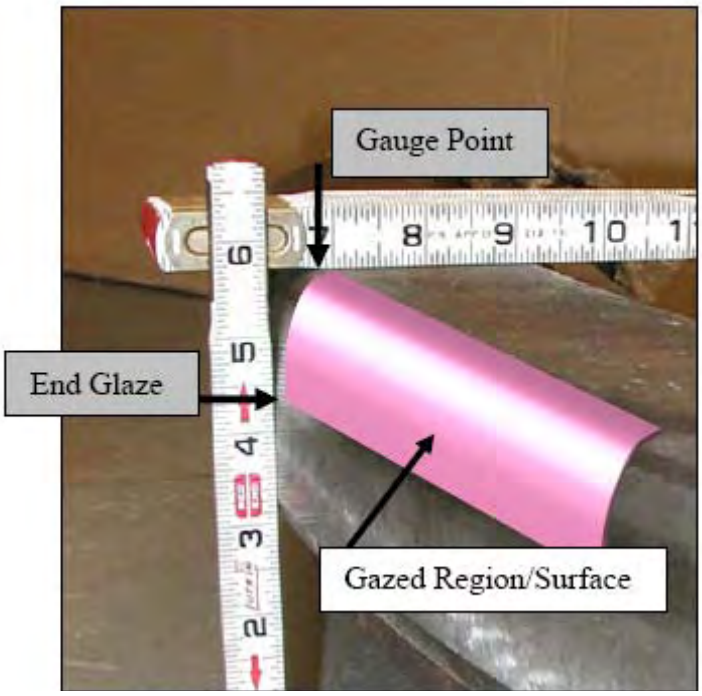

Figure 3. Glazed Region on CNRC Rim

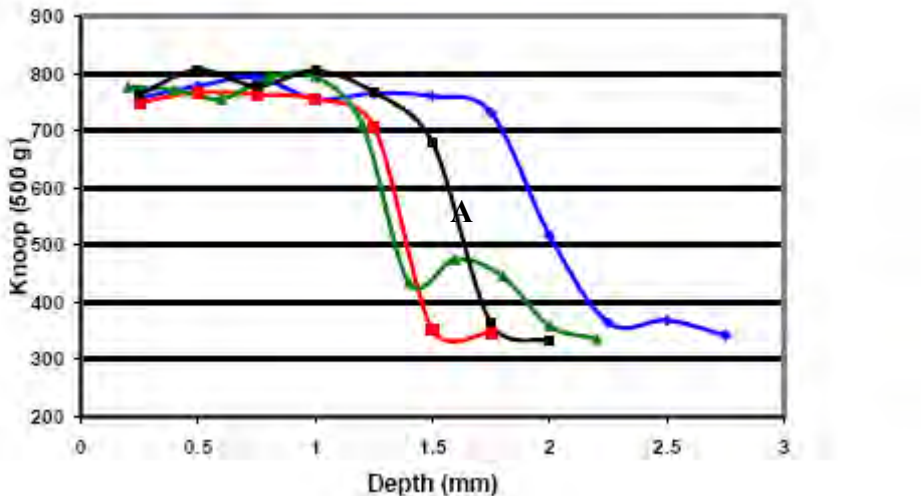

Figure 4 Knoop microhardness of CNRC rim glazed at 0.6 m/min obtained at different locations.

During cross-sectional metallographic examination of segments obtained from the sacrificial rim, several cracks were observed, as seen in Figure 5. A detailed analysis of

the cracks only occurred in overlapped (or closely-spaced glazed tracks). Figure 6 shows a Magnaflux photo of three closely spaced, but nonoverlapping laser glazed tracks. Track 1 (Figure 6) was glazed first, followed by Track 2, and finally by Track 3. As seen in Figure 6, the cracks were observed between Tracks 1 and 2, and between Tracks 2 and 3. Analysis [9] of these cracks and others that were observed in overlapped tracks revealed the cracks only occurred after the second (or subsequent tracks) were glazed (either overlapped, or closely spaced, within 0.5-1 mm).

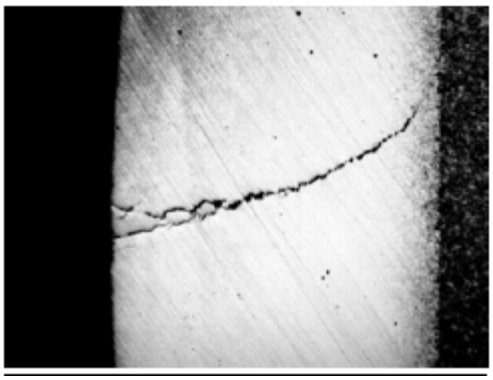

Figure 5 Optical photomicrograph of 1080 Rim material after multipass glazing treatment at 0.6 m/min.

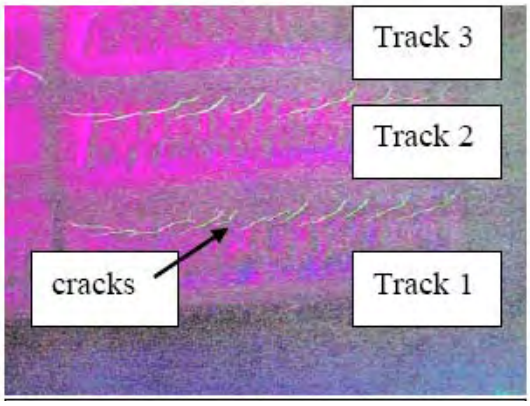

Figure 6 Magnaflux image of closely-spaced, nonoverlapped laser glazed tracks on CNRC WBB trial rim

Analysis of these cracks also revealed the following trends:

• When a region is glazed, the track consists of a well-defined region in which melting of the surface occurred, surrounded by a heat-affected zone (see Figure 7).

• Cracks form when the subsequent track is placed too close to the previous glazed track.

• The occurrence of the cracks may be significantly influenced by residual stresses in the base material (the rims used in these tests were not freshly ground; they had been used by the CNRC in previous tests and therefore contained residual stresses in the near-surface regions).

• Cracks were not observed in single, widely spaced (>1 mm) tracks, in which the heat-affected zones did not overlap.

• The occurrence of cracks in 'virgin' rail segments (Figure 7) or 1080 steel coupons was extremely rare, even in cases where the glazed regions overlapped (albeit at faster glazing speeds of 2-2.5 m/min).

The trend that NuVonyx observed in the glazed regions when tracks were either overlapped or closely spaced is shown in Figure 8. After the first pass, no cracks occur. The subsequent track (Pass 2) produces a back-tempered zone, and cracks are observed just outside of the back-tempered region in the prior (Pass 1) track. To avoid the cracks that were plaguing attempts to produce a wide (2-in.) swath of laser glazed rim (as shown in Figure 3, we decided to glaze two, approximately ½-in.-wide tracks, on the rim, with one track centered on the gauge point, and the second track spaced approximately 10-12 mm from the first track on the top of the rim.

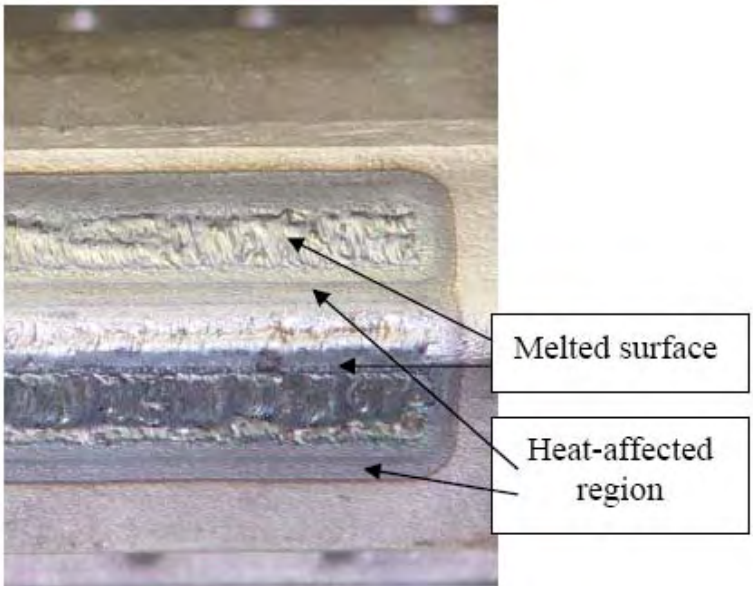

Figure 7. Photograph of glazed 'virgin' 1080 rail glazed; heat-affected zones overlapped

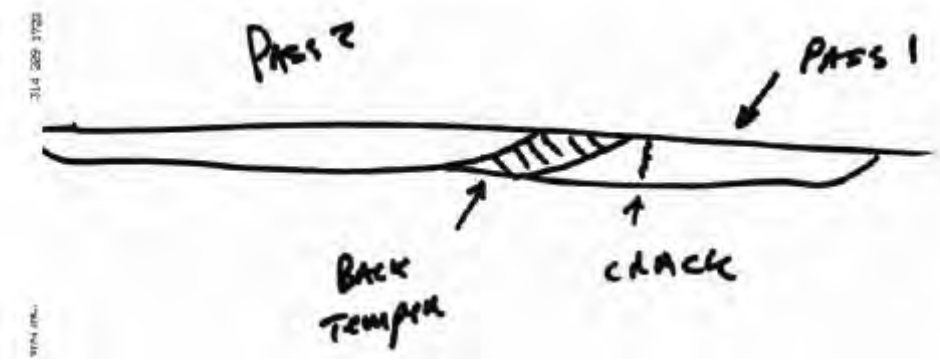

Figure 8 Schematic representation of crack location in closely spaced (or overlapped) laser-glazed tracks

To determine if moving the top-running-surface glazed region closer to the gauge glazed region would produce cracking in the region between the two glazed regions. Previously, the heat-affected zones of the gauge and top-running-surface glazed regions were separated by 10 mm. Ottawa indicated that better alignment of the top-running surface glazed region would be obtained if the top glazed region was 3 mm closer. We asked NuVonyx to perform another trial run (and Magnaflux) to determine if cracks formed

when the glazed regions were closer (approximately 7-mm separation). They performed Figure 8 schematic representation of crack location in closely spaced (or overlapped) laser-glazed tracks another run with a separation between the heat-affected zones of approximately 6 mm and no cracks were observed.

NuVonyx was given the go-ahead to treat the final rail segment if the trial runs were crack free); they subsequently glazed the final rail segment with the closer separation and magnafluxed the entire rail segment. Overall, the glazing was a success. Relatively large cracks were observed at the ends of the rail segments where they mate up with the other 180-degree segment. However these cracks are in regions that were not glazed and are believed to have been present before the glazing operation. Two very small cracks (approximately 2 mm long) were observed in one isolated region in the top running surface glazed region.

Figure 9 shows a photograph of the second rim after it was glazed; the inset shows the appearance of the two small 2-mm-long cracks that were observed in the glazed region on top of the track. Figure 10 shows a close-up of the glazed rim (mounted on the Ottawa WBB test rig). The location of the glazed tracks is also noted in Figure 10. After the glazing treatment by NuVonyx, the glazed rim was returned to Ottawa where it was reassembled with its mating rim segment and mounted on the WBB test rig.

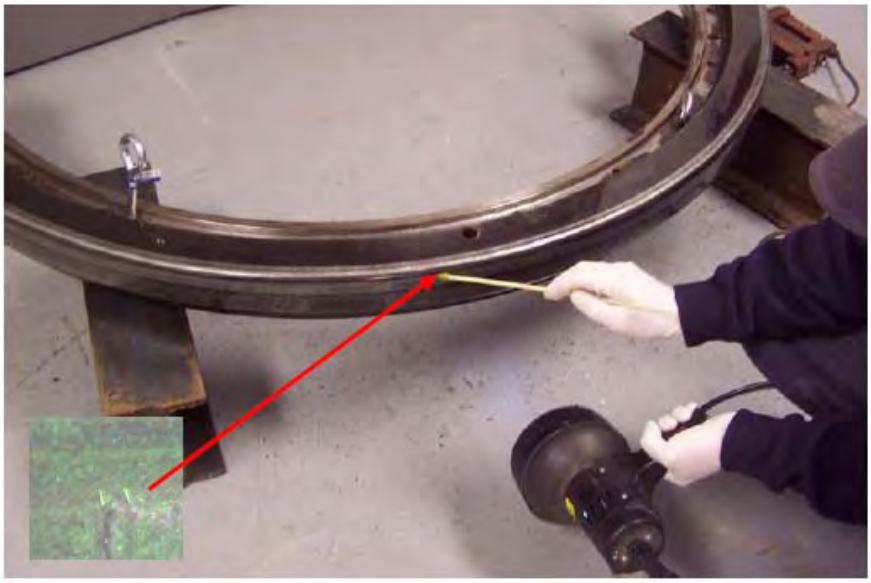

Figure 9. Photograph of glazed rim, and magnaflux image of two small cracks

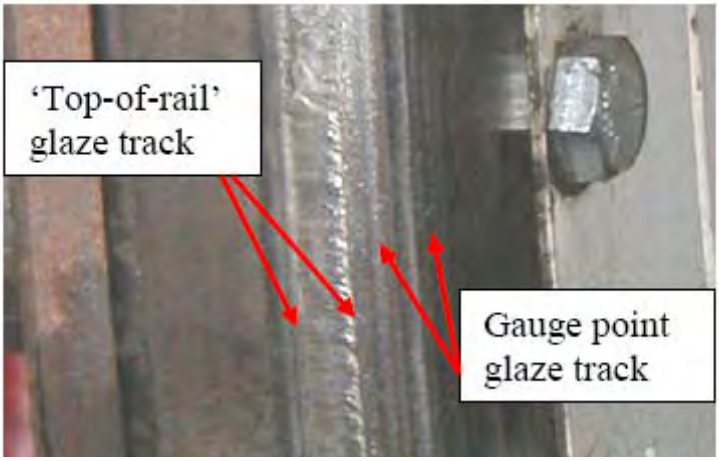

Figure 10. Close-up photograph of glazed rim

Conclusions

It was possible to optimize a large scale laser glazing process which was applied to a large rail piece. Laser glazing process will decrease rail wear and friction. However, it will result in high tensile residual stresses that will negatively affect the fatigue life of a railroad.

Also, it was shown that if the laser glazing power increased, the laser glazed layer depth will increase and the relation is reversed with the laser glazing process speed.

Acknowledgement

This work was suppo-rted by the U.S. Department of Energy, Office of Heavy Vehicle Technologies (OHVT) in Office of Transportation Technologies; Dr. Sid Diamond, Program Manager.

References:

[1] Runyon R. S., and Kumar S., 1996, "Top of Rail Lubrication", Proceedings of the Locomotives Maintenance Officers Association.

[2] Grassie S., and Kalousek J. 1997 " Rolling Contact Fatigue of Rails: Characteristics, Causes and Treatments", 6th International Heavy Haul Conference.

[3] Kumar S., Sciammarella C. A 1982, "Experimental Investigation of Dry Frictional Behavior in Rolling Contact Under Traction & Braking Conditions.", IIT TRANS-82-6.

[4] Tucker T. R. and Clauer, 1983, "Laser Processing of Materials" (MIC Report, MCIC) pp. 83-48, Metals and Ceramics Information Center.

[5] Kalker, J. J., "On the Rolling Contact of Two Elastic Bodies in the Presence of Dry Friction," M. S. Thesis, Delft, Netherlands (1967).

[6] Love, A. E. H. "A Treatise on the Mechanical Theory of Elasticity," Cambridge University Press, Cambridge, U.K. (1926).

[7] Ohyama, T., "Adhesion Characteristics of Wheel/Rail System and Its Control at High Speed," Quarterly Reports of RTRI, Vol. 33, No. 1 (1992), 19-30.

[8] Johnson, K. L. Contact Mechanics, Cambridge University Press, Cambridge, U.K. (1985).

[9] Obara, T., “The Behavior of Traction Force at Elliptic Contact between Wheel and Rail,” QR of RTRI, Vol. 36, No. 3 (1995).

[10] Kouhbor, K., "Effects of Rail/Wheel Lubrication on Reduction of Energy by Computer Simulation SIMCAR," National Conference Publication - Institute of Engineers, Australia 10th International Wheelset Congress (1992), 311-317.